PERGAMON

Renewable Energy 19 (2000) 527–543

RENEWABLE ENERGY

www.elsevier.com/locate/renene

Skytherm: an approach to year-round thermal energy sufficient houses

S. Raeissi, M. Taheri*

Chemical Engineering Department, School of Engineering, Shiraz University, P.O. Box 71345/1549, Shiraz, Iran

Received 18 January 1999; accepted 4 May 1999

Abstract

The skytherm system, a roof covered with water filled plastic bags equipped with moveable insulation, is studied and a model is presented to predict its thermal behavior. A computer program is written to calculate hourly cooling and heating load requirements of a building and is validated by comparison with field data taken from an actual house in Shiraz, Iran. This program is then used to simulate metal and concrete skytherms. It is shown that for a 140.55 m^2 one story house, the skytherm system is capable of reducing heating demands by 86% and cooling loads by 52%. © 1999 Elsevier Science Ltd. All rights reserved.

Keywords: Skytherm; Passive cooling and heating; Roof ponds

1. Introduction

For passive cooling of buildings, the roof is the part which offers the most versatile opportunities because it is the element most exposed to the sky [1]. To make use of the roof as a combined collector, storage, and heat exchanger system, Hay [2] has patented the 'skytherm' system. This system involves heating with solar energy and summer cooling to the night sky using ceiling ponds and movable insulation. Hay and Yellott [3] built a solar test room in Phoenix, Arizona, utilizing the skytherm system and tested it throughout 15 months. This

* Corresponding author. Tel.: +98-71-303071; fax: +98-71-52725.

PII: S0960-1481(99)00079-8

Nomenclature

A	surface area, m^2
C_p	heat capacity, J/kg K
CF	fraction cloud cover, dimensionless
D	instantaneous diffuse solar radiation, W/m^2
Gr	Grashof number, dimensionless
h	heat transfer coefficient, W/m^2 K
I_h	instantaneous direct solar radiation on horizontal surface, W/m^2
k	thermal conductivity, W/m K
m	mass, kg
Pr	Prandtl number, dimensionless
q	heat flux, W/m^2
q_{con}	convective heat flux from pond when panels are open, W/m^2
q'_{con}	convective heat flux from pond when panels are shut, W/m^2
Q	heat transfer rate through roof, W
R	resistance to heat transfer, m^2 K/W
t	time, s
T	temperature, K
T_{sky}	sky temperature, K
U	overall heat transfer coefficient when insulating panels are open, W/m^2 K
U'	overall heat transfer coefficient when insulating panels are shut, W/m^2 K
x	thickness, m

Greek symbols

α	absorptivity of surface, dimensionless
ϵ	emissivity, dimensionless
θ_z	zenith angle, degrees
σ	Boltzmann constant, W/m^2 K^4
$\tau\alpha$	transitivity–absorptivity product of water and bag

Subscripts

A	ambient air
B	air inside of building
C	air inside inflated air cell
F	average of inner surfaces of floor and walls
I	insulation panel
j	time increment index
LMR	lower surface of metal roof
LR	lower surface of roof
MR	metal roof

P	plastic bag
R	roof slab
S	air space between bag and insulation panel
T	waterproof sealing
UI	upper surface of insulation panel
UR	upper surface of roof
W	water (pond)

was followed by the construction of a full-sized skytherm house in Atascadero, California in 1972. Niles [4] discusses the thermal design and evaluates the performance of this house over a nine months test period. This work is focused on simulating the skytherm system numerically in order to study its efficiency for the weather conditions of Iran, in addition to determining the effects of different parameters such as the roof, water, and insulation thicknesses on the efficiency without actually carrying out expensive experimental work.

2. Skytherm system

In the skytherm system, water ponds enclosed in thin plastic bags are supported by a roof (usually a metal deck) that also serves as the ceiling of the room below. In summer, insulating panels cover the ponds during the day to protect them from the sun and heat. At night they are removed to allow the ponds to be cooled by natural convection and radiation to the cool night sky (Fig. 1). After being cooled at night, the ponds are then ready to absorb heat from the space below the following day. In winter the panel positions are reversed, as the ponds are exposed to sunlight during the day and covered with insulating panels at night (Fig. 2).

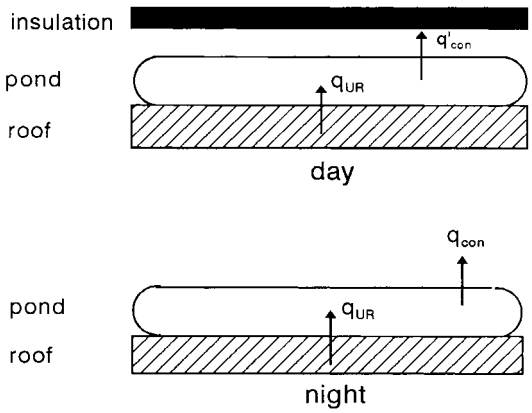

Fig. 1. Summer operation of the skytherm system.

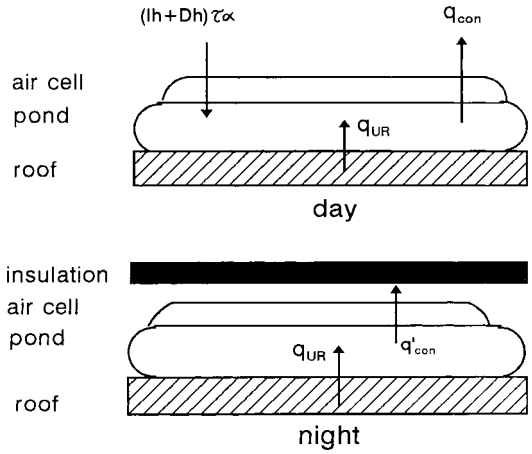

Fig. 2. Winter operation of the skytherm system.

Heat collected by the ponds is transferred from the ceiling directly to the space below [5].

The ponds are supported on a waterproofed metal or thin concrete deck. To keep the transfer of heat from the pond to the metal deck as great as possible, it is desirable to waterproof the top of the deck with a thin plastic sheet such as double laminated polyethylene carefully sealed at the edges or a fiberglass sheet and a thin coat of asphalt emulsion. Optimizing heat transfer between the ponds and the rooms requires that the underside of the deck also be used as the finished ceiling. It is important to paint the underside of the metal deck since galvanized metal is a poor radiator when bare. Because the ceiling radiates at a relatively low temperature, it can be painted any color [5].

Ponds can be inexpensively constructed by enclosing water in plastic bags made of polyethylene, polyvinyl chloride or other forms of inexpensive clear plastic. These bags may be provided with integrally connected air-cells (Fig. 2) for better efficiency. Ponds can also be constructed of metal or fiberglass tanks with rigid transparent plastic covers but these are more expensive.

The most common moveable insulation panels are 2″ polyurethane foam reinforced with fiberglass strands and sandwiched between aluminum skins. This is a standard item marketed as 'metal building insulation'. Panel tracks and supports should also be designed in a way that the panels form as tight an assembly as possible when closed [5].

3. Theoretical model

By considering the roof to be a homogeneous infinite slab, heat flow through the roof may be represented by the one-dimensional heat conduction equation as:

$$\frac{\partial T}{\partial t} = \alpha_R \frac{\partial^2 T}{\partial x^2} \tag{1}$$

where x is the distance from the outer surface to the inner surface of the roof. In a thick concrete roof, this equation must be solved numerically to obtain the temperature distribution as a function of time, but for a thin metal roof, the quasi steady-state condition is a perfect assumption. Both calculation procedures are discussed below.

3.1. Concrete roof

Assuming that the net radiation on the inner surfaces of a building is negligible, the boundary condition at the lower surface of the roof is:

$$-k_R \left.\frac{\partial T}{\partial x}\right|_{LR} = h_{LR}(T_{LR} - T_B) \tag{2}$$

where subscripts 'B' and 'LR' symbolize the air inside the building and the lower surface of the roof, respectively. At the outer surface, by assuming that there is no thermal resistance at the contacting surfaces of the plastic layer, i.e. the upper and lower surfaces of the plastic layer have the same temperatures as the water and the roof, respectively, the heat flux through the roof is:

$$q_{UR} = k_R \left.\frac{\partial R}{\partial x}\right|_{UR} = \left(\frac{k}{x}\right)_P (T_{UR} - T_W) \tag{3}$$

Subscripts 'W', 'P', and 'UR' symbolize water, plastic bag, and upper surface of the roof, respectively. In the numeric solution, the roof slab is divided into a number of nodes and its temperature profile is obtained using the Crank–Nicolson numerical approach.

3.2. Metal roof

For a thin metal roof, the above cumbersome numerical approach is not necessary due to the lower thermal resistance. But instead, radiation from the inner surface of the roof must be taken into account since roof and room temperature differences are greater in this case than for the concrete roof. Since resistances are additive, one may first define an effective thermal resistance of the roof $(x/k)_{eff}$, as follows:

$$\left(\frac{x}{k}\right)_{eff} = \left(\frac{x}{k}\right)_{MR} + \left(\frac{x}{k}\right)_T + \left(\frac{x}{k}\right)_P \tag{4}$$

Subscripts 'MR', 'T', and 'P' denote the metal roof, the waterproof sealing, and the plastic bag, respectively. Thus, the overall heat transfer coefficient between the lower surface of the metal roof and the water is

$$u_{MR} = \frac{1}{\left(\frac{x}{k}\right)_{eff} + \frac{1}{h_W}} \tag{5}$$

The resulting heat transfer through the roof is

$$Q_{MR} = A_R u_{MR}(T_{LMR} - T_W) \tag{6}$$

where 'LMR' denotes conditions at the lower surface of the metal roof and may be estimated by equating the heat transferred through the roof to the heat transferred from the room to the ceiling. This would result in the following equation:

$$A_R h_{LR}(T_B - T_{LMR}) + \frac{\sigma(T_F^4 - T_{LMR}^4)}{\frac{1-\epsilon_{LMR}}{A_R\epsilon_{LMR}} + \frac{1}{A_R} + \frac{1-\epsilon_F}{A_F\epsilon_F}} - A_R u_{MR}(T_{LMR} - T_W) = 0 \tag{7}$$

the first term accounts for convection and the second for radiation. 'F' denotes the average of the inner surfaces of walls and floor. This equation is solved by the Newton–Raphson method for T_{LMR}.

3.3. Water temperature

The water temperature required in either Eq. (3) or (6), is found using an energy balance around the water by assuming it is uniform throughout the pond (Fig. 1). When the panels are open, the heat accumulation is equal to the sum of the heat gained by solar radiation; from the roof, q_{UR}; and by convection, q_{con}

$$m_W C_{p_W} \frac{\partial T_W}{\partial t} = A_R[(I_h + D_h)(\tau\alpha) + q_{UR} - q_{con}] \tag{8}$$

I_h and D_h, the instantaneous direct and diffuse solar radiation on horizontal flat surfaces in W/m^2 are determined by the empirical equations given by Daneshyar [6] for radiation in Iran

$$I_h = (I - CF)\{951.55[1 - \exp\ |\ -0.075(90 - \theta_z)\ |]\}(\cos\ \theta_z) \tag{9}$$

$$D_h = 1.432 + 2.107(90 - \theta_z) + 121.3CF \tag{10}$$

where CF is the fractional cloud cover, and θ_x is the zenith angle in degrees.

The convective term is estimated by:

$$q_{con} = u(T_W - T_A) \tag{11}$$

Eq. (8) may be approximated to

$$T_{W_{j+1}} = T_{W_j} + \frac{\Delta t A_R}{m_W C_{p_W}}[(I_h + D_h)(\tau\alpha) + q_{UR} - q_{con}] \tag{12}$$

When the panels are shut the energy balance reduces to

$$m_{\mathrm{W}} C_{\mathrm{pw}} \frac{\partial T_{\mathrm{W}}}{\partial t} = A_{\mathrm{R}}(q_{\mathrm{UR}} - q'_{\mathrm{con}}) \tag{13}$$

where

$$q'_{\mathrm{con}} = u'(T_{\mathrm{W}} - T_{\mathrm{UI}}) \tag{14}$$

This is approximated to

$$T_{\mathrm{W}_{j+1}} = T_{\mathrm{W}_j} + \frac{\Delta t A_{\mathrm{R}}}{m_{\mathrm{W}} C_{\mathrm{pw}}}(q_{\mathrm{UR}} - q'_{\mathrm{con}}) \tag{15}$$

T_{UI} is the temperature of the upper (outer) surface of the insulating panel and is obtained by a quasi steady-state balance around the panel:

$$(I_{\mathrm{h}} + D_{\mathrm{h}})\alpha_{\mathrm{UI}} - U'(T_{\mathrm{UI}} - T_{\mathrm{W}}) - h_{\mathrm{A}}(T_{\mathrm{UI}} - T_{\mathrm{A}}) - \sigma\epsilon_{\mathrm{UI}}(T_{\mathrm{UI}}^4 - T_{\mathrm{sky}}^4) = 0 \tag{16}$$

in which

$$T_{\mathrm{sky}} = 0.0552 T_{\mathrm{A}}^{1.5} \tag{17}$$

where T_{A} is the ambient air temperature. This fourth-order equation is solved for T_{UI} by the numerical Newton–Raphson method.

Since the mode of operation of the skytherm differs in summer and winter, the heat transfer coefficients required in the above equations are obtained separately for the two seasons.

3.3.1. Summer operation

In summer the air-cells are deflated for better heat transfer at night. Also the insulating panels are opened at night to allow for radiation to the sky. The overall heat transfer coefficient between the pond and outside air will be

$$U = \frac{1}{\left(\frac{\Sigma x}{k}\right)_{\mathrm{P}} + \frac{1}{h_{\mathrm{A}}}} \tag{18}$$

During the day the pond is covered by insulating panels to prevent any solar gain by the water. The overall heat transfer coefficient between the water in the bags and the upper side of the insulation is

$$U' = \frac{1}{\left(\frac{\Sigma x}{k}\right)_{\mathrm{P}} + R_{\mathrm{S}} + \left(\frac{x}{k}\right)_{\mathrm{I}}} \tag{19}$$

where $(x/k)_{\mathrm{P}}$, R_{S}, and $(x/k)_{\mathrm{I}}$ are the resistances to heat transfer due to the plastic

bag, air space between the bag and the panel, and the insulating panel, respectively.

3.3.2. Winter operation

In winter the integrally-connected inflatable air-cells above the water are inflated for increased collection efficiency (Fig. 2). In this case, when the panels are open, the heat transfer coefficient between the water and the outside air is

$$U = \frac{1}{\left(\frac{\Sigma x}{k}\right)_{\mathrm{P}} + R_{\mathrm{C}} + \frac{1}{h_{\mathrm{A}}}} \tag{20}$$

R_{C} is the resistance to heat transfer due to the inflated air cell.

When the panels are shut the overall heat transfer coefficient between the water and the upper surface of the insulating panel is

$$U' = \frac{1}{\left(\frac{\Sigma x}{k}\right)_{\mathrm{P}} + R_{\mathrm{C}} + R_{\mathrm{S}} + \left(\frac{x}{k}\right)_{\mathrm{I}}} \tag{21}$$

4. Experimental procedure

The residential building under experiment is a one-story house with no common walls with other buildings. This case study is situated in Shiraz, Iran, at an altitude of 1491 m, latitude angle of 29.6°N and longitude angle of 52.53°E. The house has a floor area of 140.55 m^2 and a height of 3 m. Wall and window areas are given in Table 1 for each side of the building. The building is heated in winter by gas-burning heaters and cooled in summer by an evaporative water cooler.

A detailed numeric approach as reported previously [7–10] has been used to set up a computer program for simulating the thermal behavior of the house. Cooling and heating loads are calculated for each hour and summed up over 24 h to obtain the daily total cooling/heating load. Numerical values of the constant parameters used in this simulation are given in Table 1.

5. Results

The validity of the program in simulating the thermal behavior of an ordinary house has first been checked by comparing the actual heating/cooling loads provided by the heater/cooler of the test house with loads estimated by the program for a few random days in winter and summer. Good matching was observed as can be seen in Figs. 3 and 4 for winter and summer, respectively. In these figures only, actual building inside temperatures were used for estimations

Table 1
Constant values used in the simulation

Ambient air	
Average wind velocity	10 km/h
h_A	12.6 W m^2/K
Walls	
Wall thickness	0.32 m
Emissivity	0.5
Conductivity	0.89 W/m °C
Area of south facing walls	27.25 m^2
Area of north facing walls	46.10 m^2
Area of east facing walls	28.69 m^2
Area of west facing walls	32.27 m^2
Windows	
Area of south facing windows	24.62 m^2
Area of north facing windows	5.95 m^2
Area of east facing windows	7.13 m^2
Area of west facing windows	3.76 m^2
Roof and skytherm	
Thermal conductivity	
Steel roof	54 W/m °C
Concrete roof	0.721 W/m °C
Plastic bag (PVC)	0.13 W/m °C
Asphalt	0.747 W/m °C
Insulating panel	0.018 W/m °C
Thickness	
Steel roof	0.002 m
Concrete roof	0.32 m
Plastic bag	0.00045 m
Asphalt	0.00045 m
Insulating panel	0.058 m
Water	0.20 m
Transitivity–absorptivity	
Product of water-bag	0.78
h_W	$0.15(Gr_W\ Pr_W)^{1/3}k_W/x_W$, W m^2/K
Inside air	
Temperature	25°C
Number of air changes per hour	0–4
h_{LR}	
Downward heat transfer	6.1 W m^2/K
Upward heat transfer	9.3 W m^2/K

and not the chosen value of 25°C used in all the following discussions. It should also be noted that all the following results are obtained from the simulation since no field data was available for the skytherm.

The estimated hourly heat flow from the roof of the test house is given in Figs. 5 and 6 for the different roof options on 21 June and 9 February 1994,

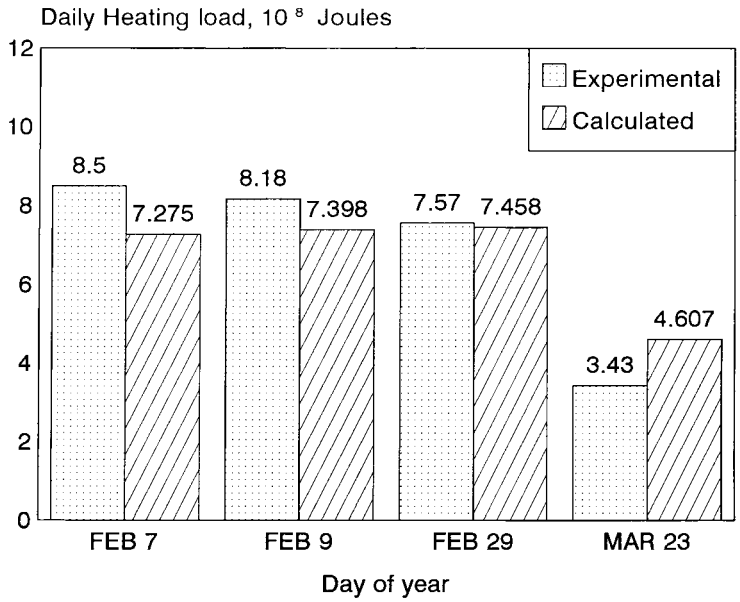

Fig. 3. Experimental and estimated daily heating loads for test building.

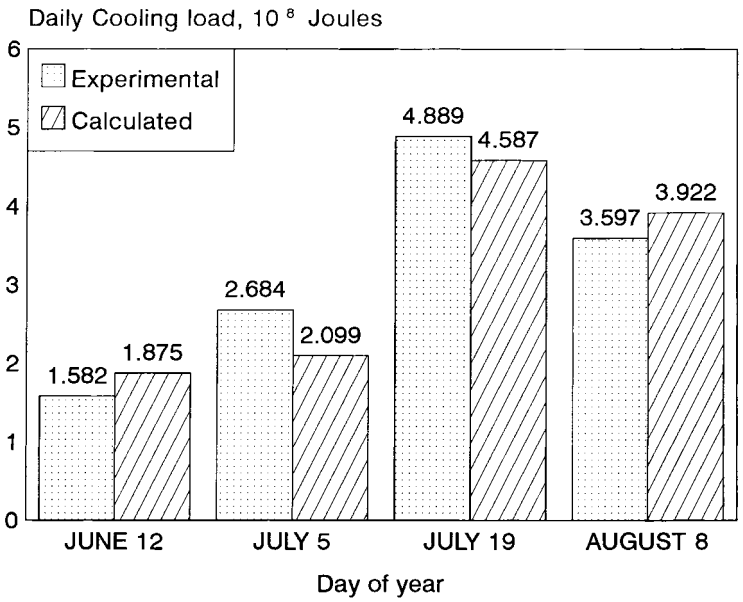

Fig. 4. Experimental and estimated daily coding loads for test building.

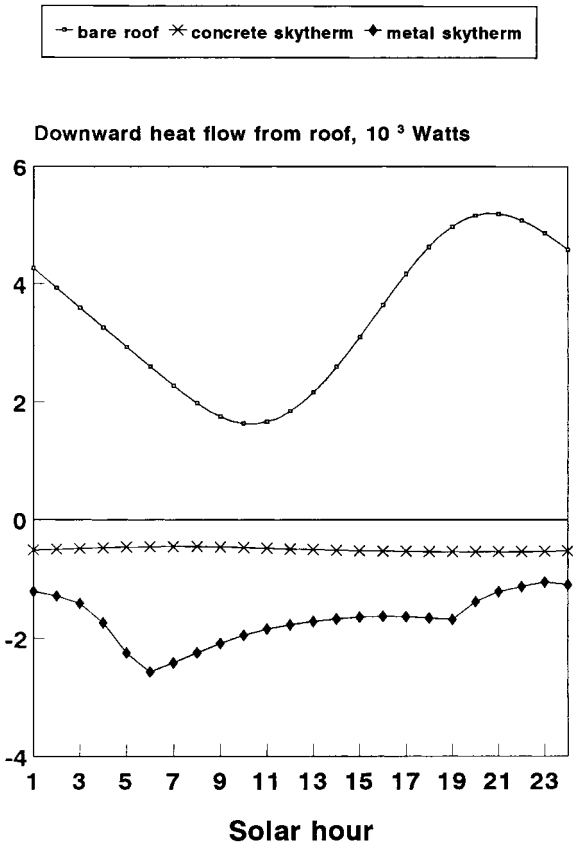

Fig. 5. Downward heat flow from different roofs on 21 June.

respectively. For summer, the bare roof shows greater variations of heat flow throughout the day as compared to the skytherm. Table 2 compares the overall daily cooling and heating loads of the house if it had either of the three types of roofs. This table shows that metal skytherms are superior over concrete ones in both summer and winter conditions. It is interesting to note that skytherms are

Table 2
Daily cooling and heating loads of test building with different roof options

Roof option	Summer (21 June)		Winter (9 February)	
	Daily cooling load, 10^8 J	Reduction (%)	Daily heating load, 10^8 J	Reduction %
Ordinary	7.45	–	5.35	–
Concrete skytherm	4.39	41.1	2.75	48.6
Metal skytherm	3.57	52.1	0.74	86.2

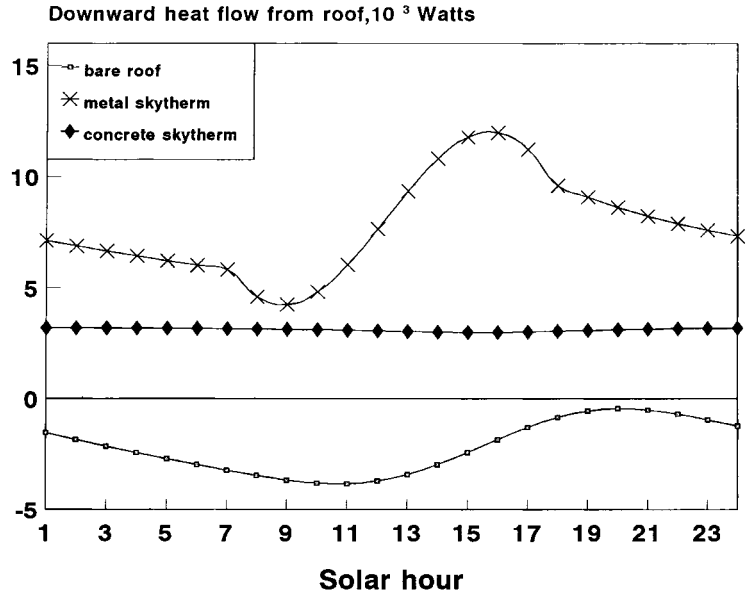

Fig. 6. Downward heat flow through different roofs on 9 February.

even more efficient in winter than summer for the climatic conditions of Shiraz, being able to reduce the heating demand by 86%.

Table 3 gives the maximum, minimum, and daily average temperature of the outer surface of the roof slab, in addition to the daily average temperature of the water and the inner surface of the roof.

5.1. Effect of roof thickness

Table 4 compares the daily energy load of the test building for two different roof thicknesses on 21 June and 9 February. In both seasons, increasing the roof thickness decreases required loads for the ordinary roof due to decreased heat flow through the roof. Thickness of the metal skytherm does not have noticeable effects on energy transfer due to the high thermal conductivity of metals. In contrast to the bare roof, the concrete skytherm shows decreased loads with thinner roofs in both seasons. As can be seen in Fig. 7 heat is continuously extracted from the concrete skytherm roof 24 h a day during the summer while the reverse is observed for winter. Thus, the smaller resistance to heat transfer for thinner concrete skytherm roofs aids the desired transfer of heat through the roof.

5.2. Effect of insulation panel resistance

On 21 June, increasing the thermal resistance of the insulating panel (thickness to thermal conductivity of panel) from 0.009 to 2.822 m^2 °C/W causes an overall

Table 3
Roof and water temperatures of test building with different roof options

Roof option		Average daily temperature, °C			Outside of roof maximum temperature, °C	Outside of roof minimum temperature, °C
		Inside of roof	Outside of roof	Water		
Ordinary roof	21 June	29.0	39.7	–	67	21
	9 February	23.3	16.4	–	41	4
Concrete skytherm	21 June	24.6	23.0	22.7	24	23
	9 February	28.6	38.5	39.9	40	37
Metal skytherm	21 June	24.6	24.6	23.6	24	25
	9 February	27.3	27.5	30.3	30	25

daily cooling load reduction of 3.2 and 10.5% for the concrete and metal skytherms, respectively. The reduction is expected but what is interesting is the difference between the trends of the curves showing the effect of the thermal resistance of the insulating panel. Fig. 8 shows this effect on the hourly heat flow from the roof for the concrete and metal skytherms. In summer, the curve of the metal skytherm is broken up into two parts; sunshine hours when the panel is shut and the different panel resistances start to show their effect as time proceeds, and dark hours when the panel is opened and the different curves start to approach each other hence, diminishing the differences caused by the panels during the day. This distinguished behavior is not seen for the concrete skytherm where a similar trend is observed for different thermal resistances. This is due to the damping power of the thick concrete roof covering up any instantaneous heat fluctuations above the roof, so that heat which passes through the roof is much more uniform. One should also note the time lag where the minimum heat

Table 4
Effect of roof thickness on daily cooling and heating load of test building for different roof options

Roof option		Daily load, 10^8 J		Addition of daily load (%)
		Roof thickness = 32 cm	Roof thickness = 5 cm	
Ordinary roof	21 June	7.45	11.82	58.7
	9 February	5.35	11.19	109.2
Concrete skytherm	21 June	4.39	3.98	−8.4
	9 February	2.75	1.60	−41.8
Metal skytherm	21 June	3.57	3.57	0.0
	9 February	0.74	0.74	0.0

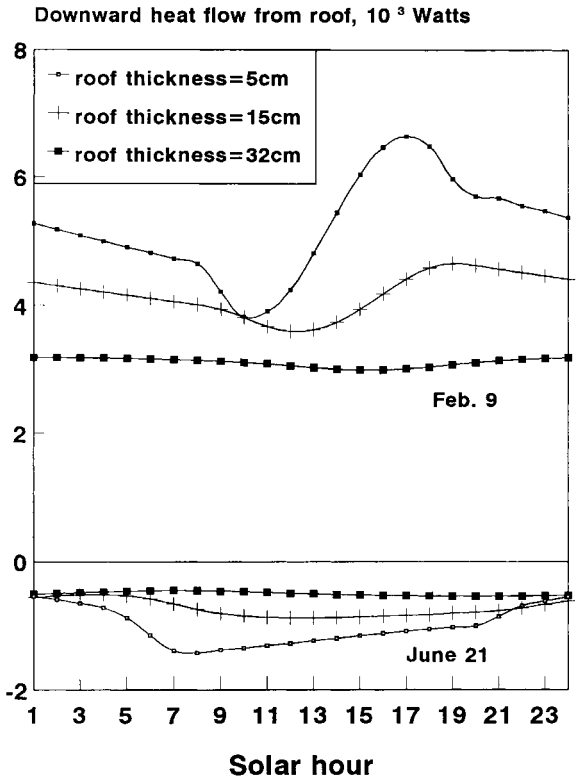

Fig. 7. Effect of roof thickness on heat flow from concrete skytherm roof.

outflow is during early morning hours for the concrete skytherm while the metal skytherm has its minimum heat outflow during late night hours.

Winter responses to different insulating resistances are similar in that the concrete skytherm dampens out the instantaneous effects which are not covered up by the metal skytherm (Fig. 8). But in this case the sunshine hours when the panels are open tend to unify the curves, while during the dark hours when the panels are shut the curves begin to separate, thus displaying the effect of the panel resistance. On 9 February, increasing the resistance from 0.009 to 2.822 m^2 °C/W causes an overall daily heating load reduction of 5.5 and 24.6% for the concrete and metal skytherms, respectively. It is seen that the effect of the insulating panel resistance is more enhanced in winter.

5.3. Effect of water height

Fig. 9 shows the effect of water height on daily cooling and heating loads for both the metal and concrete skytherms. In both seasons, as the height of water increases, the energy demands of the house decrease to a minimum, after which a

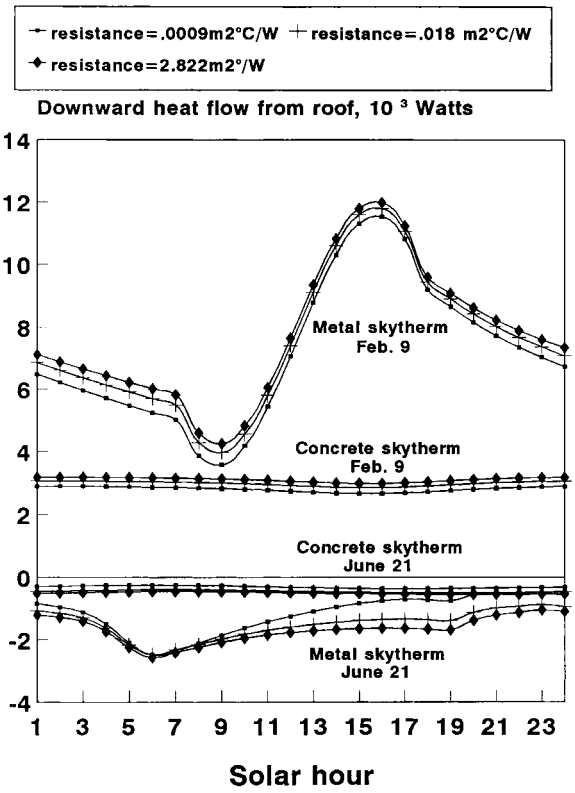

Fig. 8. Effect of insulation resistance (L/k) on heat flow from metal and concrete skytherm roof.

very slow addition of cooling/heating load is observed. This behavior is the result of interactions of the different terms in Eqs. (12) and (15) and cannot be precisely related to a specific cause. In both summer and winter, the metal skytherm is more affected by water height than the concrete skytherm in which the thick roof slab also acts as a heat storing mass thus fading the heat-storing effect of water. In any case, a pond height less than 10 cm is not recommended for metal skytherms.

6. Conclusion

The skytherm system can be very promising for reducing both cooling and heating loads of buildings in regions receiving large amounts of solar energy. For weather conditions similar to Shiraz, Iran, the thermal efficiency of the skytherm is even higher in winter than summer. In both seasons, skytherms reduce the undesired heat flow through the roof or even reverse the direction of heat flow to the desired direction. They also dampen out the great daily fluctuations of heat

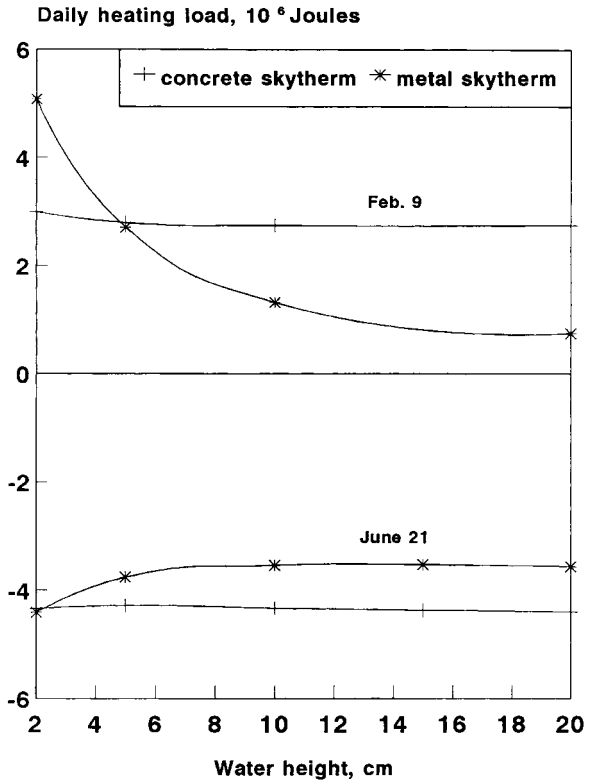

Fig. 9. Effect of water height on daily load on 9 February and 21 June.

transfer through the roof. Building the roof to be used as a skytherm of metal is more thermally effective than normal building construction material such as concrete, yet the skytherm can be quite effectively incorporated in normal existing roofs. However, it should be noted that thinner concrete roofs are better capable of reducing cooling and heating loads than thick ones.

Acknowledgements

The authors are grateful to the Research Council of Shiraz University for their financial support.

References

[1] Givoni B. Experimental studies on radiant and evaporative cooling of roofs. International Passive and Hybrid Cooling Conference, Passive Cooling. Miami Beach: American Section of the International Solar Society, 1981. p. 279.

[2] Hay HR. How to stop cooling loads before they start. Workshop Proceedings, Solar Cooling for Buildings. Los Angeles, CA, 6–8 February, 1974. p. 612.
[3] Hay HR, Yellott JI. International aspects of air conditioning with moveable insulation. Solar Energy 1969;12:427.
[4] Niles WB. Thermal evaluation of a house using a movable insulation heating and cooling system. Solar Energy 1976;18:413.
[5] Mazria E. The Passive Solar Energy Book. Rodale Press, 1979.
[6] Daneshyar M. Solar radiation statistics for Iran. Solar Energy 1979;21:345.
[7] Raeissi S, Taheri M. Cooling load reduction of buildings using passive roof options. Renewable Energy 1996;7:301.
[8] Raeissi S, Taheri M. Optimum overhang dimensions for energy saving. Building and Environment 1998;33(5):293.
[9] Raeissi S, Taheri M. Energy saving by proper tree plantation. Building and Environment 1999;34:565–70.
[10] Raeissi S, Taheri M. A study of thermal energy conservation in residential buildings in Iran. Iranian Journal of Science and Technology 1999;23(3), Transaction B.